The magnetic Compton profile of ferrimagnetic $HoFe_2$

1993 J. Phys.: Condens. Matter 5 4077

(http://iopscience.iop.org/0953-8984/5/24/009)

J. Phys.: Condens. Matter 5 (1993) 4077–4090. Printed in the UK

The magnetic Compton profile of ferrimagnetic $HoFe_2$

E Żukowski†‡, S P Collins§, M J Cooper†, D N Timms¶, F Itoh‖, H Sakurai‖, H Kawata*, Y Tanaka+ and A Malinowski‡

† Department of Physics, University of Warwick, Coventry CV4 7AL, UK
‡ Institute of Physics, Warsaw University Branch, 15-424 Białystok, ulica Lipowa 41, Poland
§ Daresbury Laboratory, Warrington WA4 4AD, UK
¶ Department of Applied Physics, University of Portsmouth, Portsmouth PO1 2DZ, UK
‖ Department of Electrical Engineering, Gunma University, Kiryu 376, Japan
* Photon Factory, KEK, Oho, Tsukuba, Ibaraki 305, Japan
+ The Institute of Physical and Chemical Research (RIKEN), Hirosawa, Wako-shi Saitama, 351-01, Japan

Received 22 February 1993

Abstract. The magnetic Compton profile of polycrystalline ferrimagnetic $HoFe_2$ has been measured at room temperature with 48 keV circularly polarized synchrotron radiation at the KEK Accumulation Ring Compton station. Although the compound has a net spin magnetic moment of less than $0.5\,\mu_B$ per formula unit it has been possible to analyse the lineshape using free-atom and free-electron momentum density distributions to yield the spin moments on the Ho and Fe atomic sites and the delocalized moment. The question of deducing orbital moments from a combination of these data and bulk magnetization results is addressed.

1. Introduction

Previous magnetic Compton scattering experiments have concentrated on elemental soft spin-dominated ferromagnets. The purpose of this investigation was to study the spin-dependent magnetic moment in a compound containing characteristically different contributions (4f from Ho, 3d from Fe, a diffuse spin moment and a very large orbital moment on Ho) in order to determine the extent to which the moments associated with individual sites could be assigned. The compound $HoFe_2$ is the first one with dominant orbital magnetization to be studied by this technique; to date, it is also the weakest magnetic scatterer studied by the Compton method. We have used these data as a vehicle to investigate the determination of both spin and orbital magnetization by combining them with magnetization results. Since this is one of the most statistically precise magnetic Compton profiles reported to date, the data analysis is carefully described.

1.1. Magnetic Compton scattering

The scattering amplitude for circularly polarized radiation, inelastically scattered (Compton scattered) from a ferromagnetic sample, can be expressed as the sum of two terms. The first describes the pure charge scattering and, by itself, yields the usual cross section expression for the Compton profile as the projection of the electron momentum distribution along the scattering vector (that expression is given in (3) below, see [1] for a general review). The second is responsible for the pure magnetic scattering; its amplitude is scaled down by a factor $|\boldsymbol{k}_f - \boldsymbol{k}_i|/mc$, where $\boldsymbol{k}_f$ and $\boldsymbol{k}_i$ are the scattered and incident beam wavevectors

0953-8984/93/244077+14$07.50

respectively. In a magnetic diffraction experiment this quantity would be fixed for each Bragg reflection, but in a Compton scattering experiment, where the momentum transfer can be varied by choice of scattering angle, θ, or incident beam energy, E_1, this can usefully be rewritten as an energy factor $g = E_1/mc^2$, where mc^2 is the electron rest energy. It is clearly a very small amplitude at conventional x-ray energies and even at the 'high' energies employed here ($g \approx 0.1$) its contribution to the cross section, proportional to g^2, can be neglected, especially when it is noted that in an incoherent scattering process, such as Compton scattering, the charge scattering, which is from all the electrons, and the magnetic scattering, which is only from those electrons with unpaired spin, are always superimposed. (Note, the situation is different for x-ray diffraction from antiferromagnets where the scattering intensities are separated in reciprocal space and effects of order $\sim g^2$ can then be observed, see for example [2]).

The cross section also contains an overlap term, proportional to g, describing the interference between the charge and magnetic amplitudes; this is generally zero because the charge and magnetic amplitudes are in quadrature, however the use of a complex polarization, namely circular or elliptical rather than linear, yields a real contribution to the scattering. Under these conditions the double differential scattering cross section can be written in the following form, similar to that given by Sakai and co-workers [3], which is based on the work of Lipps and Tolhoek [4]

$$\frac{d^2\sigma}{d\Omega\, dE_2} = r_0^2\left(\frac{E_2}{E_1}\right)[f_1 J(p_z) + f_2 g P_c S(\alpha) J_{mag}(p_z)] \tag{1}$$

where

$$f_1 = 1 + \cos^2\theta + \frac{E_1 - E_2}{mc^2}(1 - \cos\theta) + P_l \sin^2\theta \qquad f_2 = -(1 - \cos\theta)$$

and where r_0 is the classical electron radius, E_1 and E_2 are the incident and scattered photon energies, P_c and P_l are the degree of circular and linear polarization of the incident beam. The quantity $S(\alpha)$ is the geometrical spin factor which depends on the angle, α, between the incident beam and the direction of the magnetization in the sample:

$$S(\alpha) = \hat{\sigma}\left(\cos\alpha\, \cos\theta + \frac{E_2}{E_1}\cos(\theta - \alpha)\right). \tag{2}$$

The quantity $\hat{\sigma}$ indicates the magnetic field direction and changes from +1 to −1 upon reversal, causing a change in the sign of the function $S(\alpha)$ (in a fixed geometrical configuration). The second term in (1) could also be reversed in sign by changing the hand of the circular polarization. In practice the 'magnetic scattering' is isolated by reversing $S(\alpha)$ which is achieved by flipping the magnetic field since no practicable method of flipping the polarization has yet been devised; $J(p_z)$ and $J_{mag}(p_z)$ are charge and magnetic Compton profiles as defined in (3) and (4) below:

$$J(p_z) = \int\int \left(n^{\uparrow}(\boldsymbol{p}) + n^{\downarrow}(\boldsymbol{p})\right) dp_x\, dp_y \qquad \int_{-\infty}^{+\infty} J(p_z)\, dp_z = Z \tag{3}$$

$$J_{mag}(p_z) = \int\int \left(n^{\uparrow}(\boldsymbol{p}) - n^{\downarrow}(\boldsymbol{p})\right) dp_x\, dp_y \qquad \int_{-\infty}^{+\infty} J_{mag}(p_z)\, dp_z = F_S. \tag{4}$$

Z and F_S are the number of electrons and the spin moment per formula unit respectively. The arrows indicate the two possible electron spin orientations. The scattering vector,

$\boldsymbol{K} = |\boldsymbol{k}_f - \boldsymbol{k}_i|$ is chosen to lie along the z axis of a cartesian coordinate system and hence $J(p_z)$ and $J_{mag}(p_z)$ are the one-dimensional projections of the charge and magnetization density distributions onto that direction. Note that (4) contains only the spin contribution to the magnetization in the sample. It has now been confirmed conclusively that magnetic Compton scattering experiments carried out in the impulse approximation limit solely measure the spin-dependent distribution [5, 6]; this is another difference from diffraction studies, where both spin and orbital magnetization can contribute to the magnetic peaks.

The electron momentum along z is related to the scattering angle and the incident and scattered energies by the expression

$$p_z = mc\frac{E_2 - E_1 + gE_2(1 - \cos\theta)}{\sqrt{E_1^2 + E_2^2 - 2E_1E_2\cos\theta}} \tag{5}$$

where p_z is usually expressed in atomic units with $m = \hbar = 1$ and $c = 137$ (1 au $= 1.99 \times 10^{-24}\,\mathrm{kg\,m\,s^{-1}}$; on this scale the Fermi momentum in aluminium, for example, is 0.93 au). The Compton profile is normalized to the total number of target electrons (per formula unit) and the magnetic Compton profile to the number of unpaired electrons per formula unit, i.e. to the magnetic moment in Bohr magnetons (μ_B).

A 'flipping ratio', R, is defined such that

$$R = \frac{I^{(+)} - I^{(-)}}{I^{(+)} + I^{(-)}} \tag{6}$$

where $I^{(+)}$ and $I^{(-)}$ are the integrated Compton scattered intensities for opposing sample magnetizations. This is a particularly useful quantity because it reflects the strength of the magnetic scattering compared with that of the charge scattering. The numerator in (6) is proportional to the measured magnetic Compton scattering intensity as the charge scattering component does not change sign with magnetic field (or photon polarization) reversal and therefore cancels.

Although magnetic Compton scattering measurements do not measure the orbital magnetization contribution the results can, in principle, be combined with those from bulk magnetization measurements to yield both orbital and spin contributions. The practical problems associated with placing magnetic Compton profiles on an absolute scale in order to achieve this goal are discussed in detail in this paper, which also shows how the spin moments on the individual sites in $HoFe_2$ can be separated.

1.2. Magnetic moments in $HoFe_2$

$HoFe_2$ is an interesting material to investigate because the spin moment on holmium and iron sites are coupled antiferromagnetically and, although they are of similar magnitude, they are associated with 4f and 3d electrons respectively and these electrons possess quite different momentum distributions.

The expected spin and orbital moments can be predicted from Hund's rules for the Ho^{3+} ion together with neutron data. In order to preserve consistency with the sign convention used for the previous [5] studies of $HoFe_2$ the positive direction of magnetization has been taken to be parallel to the Fe moment, i.e. antiparallel to the overall direction of magnetization (spin plus orbit) which is always dominated by the moment on holmium. Given that $\mu_{Ho} = g_{Ho}\langle J\rangle\mu_B$, $g_{Ho} = 5/4$, $g_S = 1/2$, $g_L = 3/4$, $J = 8$, $L = 6$ and $S = 2$, and taking $\mu_{Fe} = 1.85\,\mu_B$ and $g_{Fe} = 2$ from low-temperature neutron data [7]

would yield an orbital moment entirely on Ho of $-g_L\langle J\rangle = -6\,\mu_B$ and a spin moment of $(-g_S\langle J\rangle + 2 \times 1.85 - 0.68) = -0.98\,\mu_B$, i.e. parallel to the overall magnetization direction; -0.68 is the estimate of the low-temperature diffuse moment [8]. The spin moment is dominated by the contribution from the Ho site, and the ratio of orbital to spin magnetization is 6.1:1.

This result can be compared with the data taken from neutron work at room temperature on a [100] single-crystal sample [9]. The room temperature moment deduced from magnetization data is $-2.73\,\mu_B$. The total moment on the Ho site is $-6.3\,\mu_B$, with $+1.85\,\mu_B$, at each Fe site and therefore a diffuse spin-like moment of $-0.13\,\mu_B$ deduced (note that this is in disagreement with the value determined in this experiment—see section 6 below). Using Hund's rule, $\langle J\rangle = 5.04$ which leads to an orbital moment of $-g_L\langle J\rangle = -3.78\mu_B$ and a spin moment of $-g_S\langle J\rangle = -2.52\mu_B$ on the holmium site. The total spin moment is therefore $(-2.52 + 2 \times 1.85 - 0.13) = +1.05\,\mu_B$, i.e. it is antiparallel to the overall magnetization direction: the ratio of orbital to spin magnetization is therefore -3.6:1 [10]. The net spin is very sensitive to the delocalized contribution; for example, the ratio -3.6:1 would become -7.6:1 if the delocalized moment inferred by Lander and co-workers [9] were replaced by the low-temperature value. Note that although $HoFe_2$ does not exhibit a compensation temperature in the usual sense of a change of sign of the *total* magnetization, it does have a *spin* compensation temperature.

Going beyond the atomic model, the magnetic properties of this intermetallic compound are determined by the exchange interaction between 4f electrons as well as 3d electrons. The magnetic coupling between 3d and 4f spins can proceed indirectly via the spin polarization of conduction electrons by the 3d moments. Another model [8, 11–13] proposes the positive polarization of the 5d electrons by the 4f moments and the antiferromagnetic coupling of the 5d moments with the 3d electrons. As the momentum distribution of the conduction and the 5d electrons differ, magnetic Compton profile analysis has the potential to discriminate between these two models.

2. Experiment

The measurements were carried out at the beam line NE1 of the Accumulation Ring at KEK in Japan [14], with the experimental setup shown schematically in figure 1. Elliptically polarized synchrotron radiation with a degree of circular polarization of about 0.6 was produced by an elliptical multipole wiggler [15]. The x-rays were monochromated with a resolution $\Delta E/E \leqslant 10^{-3}$ and focused with a water-cooled quasi-doubly bent Si [111] monochromator [16]. The incident beam, of approximate flux 10^{12} photons $s^{-1}\,cm^{-2}$ at a sample position, was adjusted to a vertical height of 1.5 mm and a width of 9 mm. The incident beam energy was chosen to be 48 keV, i.e. below the Ho K-shell absorption edge, in order to reduce K-shell fluorescent contributions. They cannot be avoided entirely since the higher-energy photons passed by the third harmonic of the monochromator add a small parasitic contribution.

A polycrystalline sample of a ferrimagnet $HoFe_2$ was made from high-purity materials, thereby minimizing the contamination of the Compton spectra with rare-earth K-shell fluorescent lines. The sample was cut to a rectangle of size of 24 mm × 9 mm × 1 mm thick, and clipped to the pole pieces of a C-type electromagnet. With the sample removed the magnetic field in the centre of the 20 mm air gap between the pole pieces was at most 0.15 T [17]. The angle between the incident beam and the sample's magnetization (parallel to the surface and the longer side of the sample) was set to 10°. The electromagnet had

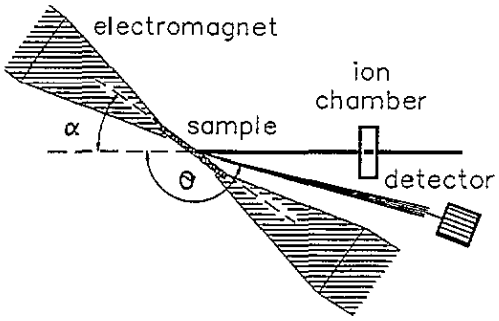

Figure 1. The experimental geometry. θ is the scattering angle, α is the angle between the incident wavevector and the direction of magnetization in the sample. The sample was clipped to the poles of the electromagnet and the radiation scattered from the $HoFe_2$ sample was detected by the 13-crystal germanium detector. The direction of magnetic field was reversed every 5 s.

been designed with two priorities: firstly to ensure that a large angle of scattering was possible, in order to maximize the momentum resolution of the measurement, and secondly to permit a small value of α, thereby maximizing the magnetic effect—see (1) and (2). A stronger 'standard' electromagnet, with larger pole pieces, could not be used because the pole pieces would have obstructed the scattered beam (see figure 1). The magnetic field from the electromagnet's tapered pole pieces, coupled to the sample, was sufficient to magnetize the material to at least 85–90% of its saturation value, as will be shown later.

The scattered radiation was detected by an integrated set of thirteen intrinsic germanium detectors cooled by a common liquid nitrogen dewar; the detector head was positioned about 1 m from the sample. The detectors present a total surface area of about $66 \times 34\,mm^2$ [18], the average scattering angle being 160° and ranging from 158°–162° for the outside detectors in the horizontal scattering plane. Each detector had its own power supply, amplification chain and fast (200 MHz) ADC; each spectrum was recorded separately in a computer-based multichannel analyser with separate memory channels for each magnetization direction. The amplifier and ADC gains were carefully adjusted to place the elastic peaks at the same channel. The counting rate per detector was below 25 000 CPS (i.e. about 300 000 CPS in the whole system) at an initial ring current of 25–30 mA. One ADC from the system was connected to an ionization chamber that monitored the primary beam intensity. The ionization chamber output and the intensity of the elastically scattered line were used to normalize the data.

The spectra were collected in the sequence [+, −, −, +] with 5 s dwell time and 1 s between each interval; (+) and (−) indicate the two opposite directions of the magnetizing field. We shall refer to the (+) direction as the 'spin up' or the 'positive' spin orientation which produces 'spin up' or 'positive' data, and vice-versa for the (−) direction. The frequent switching of the magnetization helped to average out the effects of the ring current decay, which occurs with a lifetime of about 4–5 h. However it does not average fast beam fluctuations, and some monitoring of the beam intensity, as was mentioned above, was necessary. The measurement was carried out over 2.5 days and the Compton profiles were collected during 30 h of useful beam time. (The discrepancy between these figures arises from the fact that the Accumulation Ring is not a dedicated source of synchrotron radiation: it is used as an injector into the TRISTAN 30 GeV ring.) An integrated Compton intensity of approximately 10^{10} counts in the region from −10 au to +10 au was obtained; of this less than 0.04% was magnetic in origin.

The energy resolution of each detector was deduced from the widths of the elastic peaks. The average FWHM of the elastic peaks was 445 eV at 48 keV with a small variation of ±20 eV for the individual detector crystals. This corresponds to a resolution of 0.82 au in momentum space and this value was used for the overall profile resolution with negligible

error. Twelve independent detector channels were used to acquire data. Each set was processed separately and checked for irregularities before being combined with the other eleven.

3. Data analysis

The data analysis takes into account the following factors: (i) beam intensity fluctuations, (ii) energy-dependent corrections for absorption of the beam in the sample and for the energy dependence of the Compton cross section and (iii) the effect of multiple scattering. It is then possible to discuss (iv) the symmetry of the magnetic Compton profile as an indicator of the quality of the data and (v) the problem of establishing an absolute scale for the magnetic profile. A brief description of all these points is given below.

3.1. Beam fluctuations

Fluctuations of the incident monochromated beam as well as its steady decay, were monitored by an ion chamber. The ratio of the ion chamber counts for spin-down and spin-up orientations should ideally have been unity; in fact it was 1.0002, which serves to illustrate the stability of the beam. The value was used to correct the counts in all 12 negative spectra to ensure that these data were scaled to the same beam intensity as for the positive data. This correction, although small, can alter the peak height of the magnetic Compton profile by about 1%, since the magnetic modulation is similarly small ($\approx$0.04%). Using the elastic or fluorescent peak areas for data normalization gave a very similar correction factor (they differ by less then 3%).

3.2. Energy-dependent corrections for absorption and the scattering cross section

The absorption in the sample is significant. The mean free path for the incident beam (48 keV) was 200 μm, decreasing to 90 μm in the low-energy region of the profile (35 keV). This resulted in a 30% reduction in count rate at 35 keV relative to the Compton peak value at 40.6 keV and a 15% increase at 45 keV.

The magnetic Compton cross section calculated by Lipps and Tolhoek [4] was used together with the relativistic Compton cross section for charge scattering [19]. The effect of the energy dependence of the magnetic cross section, relative to the Compton peak count rate, was a 25% reduction in count rate at 35 keV and a 15% increase at 45 keV. For the charge cross section these factors are 10% and 5% respectively.

3.3. Magnetic multiple scattering

The Monte Carlo simulation of the magnetic Compton scattering from iron developed by Sakai [20] has been generalized to deal with any composition of magnetic material and used to determine the magnetic multiple scattering contribution in this study of $HoFe_2$. The ratio of double to single magnetic scattering was calculated to be 1.7% for an iron sample under the present conditions; for the $HoFe_2$ sample, where photoelectric absorption is more severe, this ratio is significantly less than 1% and smaller in magnitude than the statistical accuracy of these data. For these reasons no corrections for multiple scattering were made to either the magnetic Compton profile or the total profile. It should be noted that at higher incident energies the photoelectric absorption cross section is reduced and the effect of magnetic multiple scattering on the difference profile must be taken into account.

3.4. The asymmetry of the profiles

After the corrections for the energy dependence of both the sample absorption and the scattering cross sections the scattering angle was calculated from the position of the Compton peak and the data were converted to a momentum scale. The Compton profiles were then normalized, taking account of the fact that not all the K-shell electrons of holmium, plus some of K-shell electrons of iron and L-shell electrons of holmium, can scatter inelastically in this experiment because the energy transfer is less than their binding energies. A free-atom Compton profile [21], smeared with the experimental resolution gave a profile area of $A_{HoFe_2} = 99.49$ electrons in the range from -10 au to $+9$ au (the high energy is limited to $+9$ au to exclude the region where the Ho Kα_2 line lies). The normalized charge and magnetic profiles, expressed as a percentage of the integrated charge Compton profile, are shown in figures 2 and 3 respectively; the normalization procedure will be discussed later.

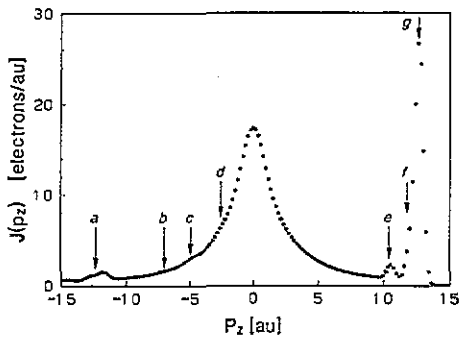

Figure 2. The total (charge plus magnetic) Compton profile of $HoFe_2$ displayed over an extended range of the momenta to show the parasitic contributions. The Ho Kα_2 (*e*), Ho Kα_1 (*f*) and the elastic line (*g*) are above +10 au. Weak fluorescence from cerium impurities is situated below -10 au (position *a*) and around -2.5 au (position *d*). Small features at *b* and *c* are detector escape peaks from the elastic line and holmium fluorescence. The estimated background was less than 3% of the total Compton profile.

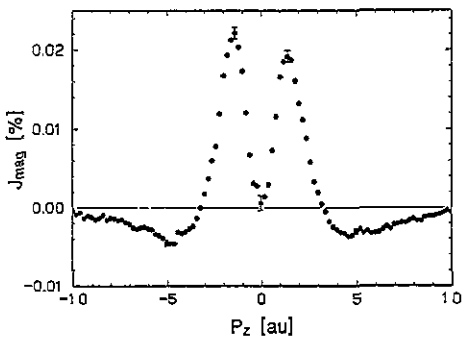

Figure 3. The magnetic Compton profile of $HoFe_2$. The intensity scale is presented as a percentage of the total profile. For comparison, the magnetic Compton profile of iron would be entirely negative with this sign convention. Small distortions from the smooth curve in the profile around -4.5 au are related to imperfect cancellation of the detector escape peaks from elastic and holmium fluorescent radiation. The only asymmetry appears to be the unequal peak heights at 1.5 au. The left/right side-averaged magnetic Compton profile is presented in figure 6.

The total Compton profile, shown in figure 2 is well separated from fluorescence contaminations (Ho Kα_2 and Ho Kα_1) are labelled *e* and *f* respectively. The elastic line, labelled *g*, is at 12.5 au and the very weak Kα fluorescence from rare-earth cerium impurities (labelled *a*) is situated outside the specified momentum range; cerium Kβ fluorescence (labelled *d*) is negligible. The Ge K escape peaks, associated with the elastic scattering, and holmium Kα fluorescence are labelled *b* and *c* respectively. The escape peak associated with the Compton line itself has an energy lower than the displayed range.

Apart from these parasitic contributions, the asymmetry of the profile did not exceed 1% of the profile maximum and is negligible in the high-momentum region; this confirms the validity of the energy-dependent corrections. The data were not corrected for any background contribution because no simple measurement of it is possible. The background was, however, deduced assuming that the charge profile at high momenta, say $|p_z| \geqslant 5$ au, must follow the free-atom profile of $HoFe_2$. The contribution so derived did not amount

to more than 3% of charge scattering. In any event the background is not dependent on magnetic field direction and subtracts out of the magnetic profile; it does, however, reduce the value of R (6) by about 1%.

The magnetic Compton profile (figure 3) has a very deep hollow at its centre and takes negative values at momenta above 3 au. Its area, as defined by (6), is only $R_{HoFe_2} = 0.037(2)\%$. For comparison, the same ratio for ferromagnetic iron is 1.022(9)%. This is explained by the smaller net spin moment in $HoFe_2$ coupled with the larger total number of electrons. However, a small net moment does not necessarily imply a small magnetic Compton profile. As figure 3 clearly shows, there are significant positive and negative contributions to the lineshape which derive from the antiferromagnetic coupling of the spins on the two sites. The lineshape analysis is presented in section 5.

The magnetic Compton profile, within statistical error, is generally symmetric, which confirms the validity of the energy-dependent corrections. Apart from the escape peaks, which can be reliably removed, there is only one significant asymmetric feature, a difference in peak height of three standard deviations at around 1.5 au which has no obvious explanation in terms of parasitic effects. It does not appear to be due to multiple scattering, which is estimated to be too weak to explain this feature. The profiles were finally left/right averaged to improve statistical accuracy and to eliminate any residual corrections that are linear in the photon energy.

4. Sample magnetization and normalization of the magnetic profile

In order to interpret the data on an absolute scale it is necessary to determine the magnetization in the sample. Two complementary measurements of the magnetization in $HoFe_2$ exist. The first is a neutron diffraction measurement of a $HoFe_2$ single crystal [9] and the second is a magnetization measurement by means of a magnetic balance, which was performed on a small sample taken from the same polycrystalline plate as was used in this experiment. The neutron data, after spherical averaging, predict the saturation magnetization to be 2.96(5) μ_B at 4.6 T; at 1.6 T it is 2.69(5) μ_B; both figures are for room temperature. The magnetic balance datum deduced from measurement up to 1.3 T was 2.90(5) μ_B, which is in good agreement with the value 2.87(5) μ_B taken from Burzo [22].

There is no precise estimate of induction inside the sample fixed between pole pieces of an electromagnet in the manner shown in figure 1. To overcome this uncertainty the magnetic scattering was measured in three test runs at reduced electromagnet current: $I_1 = \frac{1}{2}I_{max}$, $I_2 = \frac{1}{4}I_{max}$ and $I_3 = 0$ A, where $I_{max} = 2.4$ A indicates the maximum available electromagnet current used in all runs of the experiment. The results are shown in figure 4. It is evident that, even for a magnetic field reduced to 25% of its maximum, the magnetic effect is only slightly diminished. In each case the areas of the magnetic Compton profiles are proportional to the sample magnetization. From a knowledge of the magnetization curves, which are not reproduced here, this simple test indicates that the sample was close to saturation, with a magnetization of at least 85–90% of the saturation value.

The normalization of the magnetic Compton profile to the net number of unpaired electrons also requires information about the polarization of the incident beam. This cannot be easily measured directly and a measurement on a reference sample with a well known moment, namely iron, was preferred. The magnetic effect in a fully saturated pure iron sample was measured under identical conditions to the $HoFe_2$ experiment and, assuming a spin moment μ_F of $-2.1\,\mu_B$ for the electrons in iron in the momentum integration range from -10 au to $+9$ au, the polarization factor could be determined. (Note that the spin

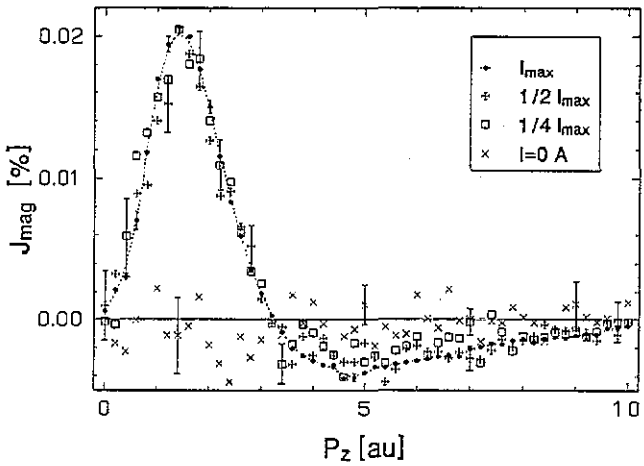

Figure 4. The magnetic Compton profile of $HoFe_2$ measured at different magnetic fields. It is evident that, even for a magnetic field reduced to 25% of its maximum, there is still a significant magnetic signal (more than 80% of that measured at $I_{max} = 2.4$ A, the maximum available electromagnet current). This supports our assumption that the sample was close to saturation when the maximum possible field was applied. The magnetic origin of the effect is confirmed by the absence of any significant signal at zero field.

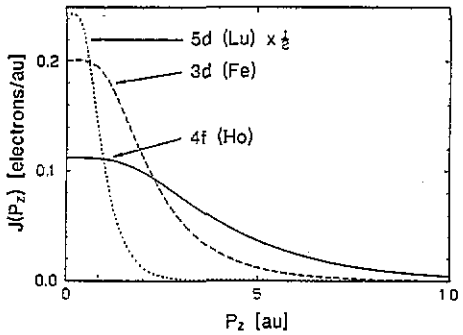

Figure 5. Atomic Compton profiles of 3d iron and 4f holmium electrons [21]. The average value from spin-up and spin-down, $4f^{(+)}$ and $4f^{(-)}$ respectively, relativistic calculations in the case of 4f electrons was used in the fits of these atomic Compton profiles to the experimental data. The 5d electron atomic profile taken from lutetium as a nearest neighbour of holmium is also plotted (scale reduced by 50%). The shape of this profile for momenta below 1 au is very close to the parabola used to represent the diffuse moment and is discussed in the text.

moment in iron is parallel to the magnetic field and therefore negative in our convention). The same data analysis procedures gave $R_{Fe} = -1.022(9)\%$. The scattered intensity was more intense from iron than that from $HoFe_2$ because of lower photoelectric absorption.

The final normalization factor for $HoFe_2$ was calculated from the relation

$$\mu_{HoFe_2} = \mu_{Fe} \frac{A_{HoFe_2}}{A_{Fe}} \frac{R_{HoFe_2}}{R_{Fe}} \tag{7}$$

where μ is the net spin magnetization of the samples; the value in Bohr magnetons is the normalization integral for the magnetic Compton profile. The quantity A is the number of electrons contributing to the total inelastic scattering and is somewhat less in value than the atomic number Z because of the limited range of integration of the Compton profile. In the chosen momentum range from -10 au to $+9$ au, $A_{HoFe_2} = 99.49$ electrons, $A_{Fe} = 23.64$ electrons.

Using the above data gives a spin moment $\mu_{HoFe_2}/\text{spin}/ = 0.32(2)\,\mu_B$ ($0.31(2)\,\mu_B$ in the symmetric region from -10 au to $+10$ au).

5. Compton lineshape analysis

It should be emphasized that the lineshape can be analysed into the *relative* contributions from different sites *without* any normalization of the profile. The normalization discussed above is only needed in order to place absolute values on the spin moments and then, by combination with magnetization data, to determine the orbital momentum contribution. We turn first to the analysis in terms of these relative contributions. The profile shown in figure 3 has been analysed in terms of atomic and free-electron momentum distributions. This basis was used successfully in earlier work to determine the localized and itinerant magnetic moments in ferromagnetic Gd [23] and ferrimagnetic amorphous $Gd_{60}Fe_{40}$ alloy [17]. It was also used to investigate the charge transfer in Co–Ni–B and Fe–Ni–B amorphous alloys [24, 25]. In all cases the tabulated free-atom Compton profiles compiled in [21] were used for the 3d electrons in iron and the 4f electrons in holmium. The Compton profiles associated with these atomic momentum distributions are shown in figure 5, together with a 5d profile that will be discussed later; all the Compton profiles differ greatly. Given that these 3d and 4f functions constitute an adequate starting point they can be used to fit the data and the fitting parameters will indicate the relative moments.

Inspection of figure 3 shows immediately that 3d and 4f functions alone are not sufficient to describe the sharp central minimum in the profile. The magnetic Compton profile of iron and other transition metals show similar 'volcanic' features, which are due to 4s, p delocalized electrons spin polarized negatively with respect to the spin moment on the transition metal site [26]. If it is assumed that the central dip in this magnetic Compton profile has the same origin, then to a first approximation its momentum can be described by a free-electron gas and its Compton profile is therefore a parabola which is cut-off at the Fermi momentum [1]. This function was added to the 4f and 3d free-atom profiles of [21] and each was convoluted with the experimental resolution (i.e. a Gaussian of full width at half maximum of 0.82 au) and then the data were fitted by the least squares technique. The excellent fit is shown in figure 6 by the full curve which passes, almost exactly, through the experimental points. The inset shows all the functions in full.

Fitting the data with a parabola in which the Fermi 'cutoff' momentum, p_F, as well as its height are free parameters is not entirely justified: the Fermi momentum should be determined by the density of the delocalized negatively polarized electron gas. In this analysis it is not: the refined value is p_F=1.3 au, which is too high. Even if all the 4s, p electrons in $HoFe_2$ are assumed to be free electrons, the calculated p_F cannot exceed 0.8 au. The free-electron model is clearly inadequate. In fact, since the magnetic Compton profile is the difference between majority and minority profiles, any free-electron contribution will correspond to a difference between two free-electron-like distributions rather than a simple parabola: however, this will still have a similar width with a cutoff at the characteristic Fermi momentum, and at the resolution of this experiment such subtleties will not be detectable. Whatever band model might be invoked for the delocalized electrons it will have to reproduce a lineshape that is (before deconvolution) a good approximation to a parabola at this level of accuracy. The 4f and 3d momentum distributions lead to Compton profiles that are so much broader than the central dip that the exact choice of basis function for the latter does not significantly affect the relative moments apportioned to the 4f, 3d and diffuse contributions. It is likely that a band calculation would produce a slightly different 3d profile at low momenta (say below 2 au), but that the 4f free-atom-like profile would be unchanged.

In order to explore further the problem of fitting the central dip we considered the explanation of extra diffuse magnetization proposed by Boucherle and co-workers [12] and

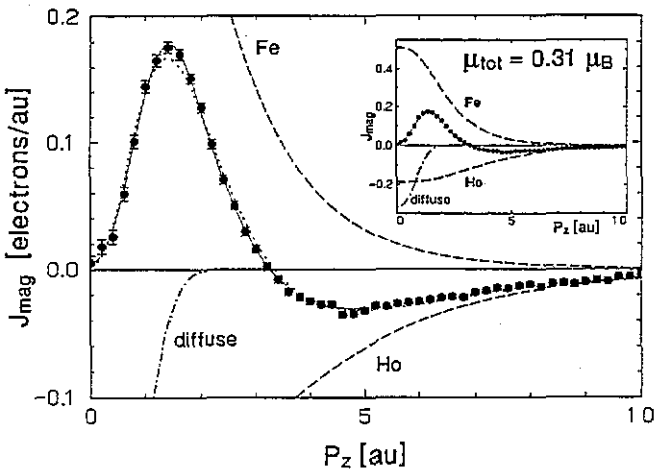

Figure 6. Lineshape analysis of the magnetic Compton profile of $HoFe_2$. The full circles represent the left/right experimental data, normalized to 0.31 electrons, which is calculated from the reference measurement on an iron sample. The broken curves show the appropriate atomic profiles indicating the relative contribution of these profiles (3d upper, 4f lower curve) to the total. The chain curve shows a parabolic free-electron-like profile describing the diffuse spin contribution. All models have been convoluted with the experimental resolution function. The fit with a 5d lutetium profile (taken from lutetium, the nearest neighbour of holmium) is shown by the dotted curve. The inset shows the full range of the fitting.

Brooks and co-workers [8, 13], in which the electrons are associated with the rare earth site. They proposed that, in contrast to the transition metals where the non-3d magnetization is almost constant in the cell, the additional magnetization density is centred on the rare-earth atom and the electrons polarized by the 4f moments have an atomic 5d character common to a wide range of rare earth compounds. In order to test this in a very approximate manner the 'volcano' was fitted by a 5d atomic profile instead of a parabola. Lutetium was chosen because it is the nearest neighbour of holmium for which the 5d Compton profiles are available [21]. This fitting is shown in figure 6 by a dotted curve. It is close to the data points, which means that the 5d function has the correct characteristic momentum distribution to describe the major component of the diffuse moment that is consistent with the modelling of the magnetization density in several Laves phase compounds [8]. The residual difference, which might be different if a more appropriate 5d function was available, should correspond to any 4s, p delocalized density. Clearly, at low momentum the magnetic profile requires a more sophisticated description than is provided by either free-electron or free-atom functions, and these data should provide sufficient incentive for this to be pursued.

6. Determination of magnetic moments

The magnetic moments derived from the fit are listed in table 1. The first set of data (column A) corresponds to the measured spin moment μ_{HoFe_2}/spin/= 0.31 μ_B, as was estimated from the normalization procedure reported in this paper. We know that this only corresponds to approximately 85–90% of the saturation magnetization of the sample measured at fields up to 1.3 T. Given the imprecision in this latter figure it does not make sense to use these values directly as a basis for estimating the orbital moment on the Ho site. If, in future

experiments, the magnetization in the sample is measured directly under actual experimental conditions, this problem can be overcome and all the individual moments, corresponding to any chosen value of magnetization, will be determined by simple scaling.

Table 1. Magnetic moments determined in the magnetic lineshape analysis of $HoFe_2$. The values listed in the first column (A) relate to the total spin magnetization measured in this work. Columns B and C relate to the magnetic Compton profile data with the moment on the iron site fixed at $1.7\,\mu_B$ [22] (column B) and $1.85\,\mu_B$ [8,9] (column C). Column D has the moments predicted from room temperature neutron measurements on a single crystal sample [9] and the spin and orbital moments on the Ho site have been split up by the application of Hund's rules. In columns B, C and D the total moment is derived from both magnetic balance and neutron magnetization measurements. μ_{Ho}/orbital/ is calculated by subtraction of the spin moments from the total moment.

	A	B	C	D
μ_{Fe}	1.27(2)	1.70	1.85	1.85
μ_{Ho}/spin/	−1.64(2)	−2.19(3)	−2.38(3)	−2.52(4)
μ_{HoFe_2}/spin/	0.31(2)	0.41(3)	0.45(3)	1.05(16)
μ/diffuse/	−0.59(2)	−0.80(3)	−0.87(3)	−0.13(15)
μ_{HoFe_2}/total/	—	−2.90(5)	−2.90(5)	−2.73(5)
μ_{Ho}/orbital/	—	−3.31(6)	−3.35(6)	−3.8(2)

The second set of data in the table (column B) correspond to fixing the moment on each iron site at μ_{Fe}/spin/= $1.70\,\mu_B$; there is considerable evidence for this value in a number of low-temperature magnetic studies of a whole range of rare-earth iron compounds [22]. Furthermore, the moment on the Fe site is not expected to soften in the manner that the Ho moment does and so, if this value is accepted, it should correspond to scaling these data to the equivalent of a fully saturated sample. The other spin moments are related to the measured data by simple scaling and it is now possible to combine the scaled spin data with the magnetic balance data to estimate the Ho orbital moment. The value assumed by Lander and Gregory [9] for the Fe moment was the higher value of μ_{Fe}/spin/= $1.85\mu_B$. This value leads by a similar scaling to the figures in column C. Finally, these data are compared with the moments predicted from room temperature magnetization measurements and the neutron data (column D); in that case the spin and orbital moments on the Ho site have been split up by the application of Hund's rules.

Too much should not be read into the moments deduced from this magnetic Compton scattering experiment since the sample magnetization was not known with great precision. However, the above analysis shows how individual spin and orbital moments can be separated in such an experiment. The values obtained only differ from the neutron data in one significant aspect, namely the room temperature diffuse moment. This difference is not sensitive to the method by which the moments have been deduced; the values in columns A, B and C range from 0.59–$0.87\,\mu_B$, which is somewhat higher than the estimate of Lander and Gregory [9]. The value reported here is much closer to the low-temperature prediction of $0.68\,\mu_B$ [8], implying that the diffuse moment is not strongly temperature-dependent, as expected.

7. Conclusions

The characteristic difference between the momentum distributions of the electrons contributing to the spin moment in $HoFe_2$ allows the *relative* spin moments to be assigned

with comparative ease and this, in itself, is a considerable triumph, especially when it is recalled that the magnetic effect is of order 0.04% of the charge scattering. The uncertainty between the absolute values quoted here illustrates some of the experimental problems. In the first place, it was not possible to saturate fully the sample with the electromagnet at our disposal; the moments in column A are therefore not saturation moments and as such are not directly comparable with other results. It will be possible to improve on this situation in future measurements at the KEK Accumulation Ring, at least for room temperature measurements, following the installation of a superconducting magnet capable of fields in excess of 1 T at the sample. At lower temperatures, where many of these materials become significantly harder magnetically, there still may be problems associated with developing the full moment in the sample. In these measurements, which were intended to provide information about the magnetic lineshape, the magnetization within the sample was not known with sufficient precision to permit simple scaling of the data: instead certain assumptions about the moment at the Fe site were invoked. This apart, as long as a 'standard' spin-dominated ferromagnet can be measured with adequate accuracy to provide a calibration standard the data can be placed on an absolute scale, independent of any assumptions about individual moments. Since experiments on samples such as soft iron are much easier than the one attempted here, this should not be a problem.

We believe that the magnetic Compton scattering technique, as detailed in this paper, will become sufficiently precise to enable spin moments to be measured and orbital moments deduced with enough accuracy to make them valuable. However, the magnetic Compton method does not just yield net moments, they are merely the integrals of the profiles that are measured and the latter are of considerable intrinsic interest. The magnetic lineshape reported here is surprisingly well fitted by free-atom functions at high momenta, but the fits proposed at low momenta require further justification in terms of band theory. In particular, it is possible that a band calculation of the low-momentum part of the 3d-like density could diverge significantly from free-atom behaviour; in that case the diffuse moment deduced from the fitting could be rather different. We shall investigate this in future work.

In future experiments we plan not only to establish the absolute scale with greater accuracy than was attained here, but also to study the temperature variation of the spin moment and follow its reversal with lowering temperatures as the holmium (or other rare-earth) moment increases. A report of such a result, recently obtained, will be published elsewhere.

In general, these magnetic lineshapes should provide a probe of the nature of the diffuse moment in particular and a general test of the adequacy of band theoretical descriptions of the charge density in these materials.

Acknowledgments

We are grateful to the UK Science and Engineering Council and the British Council (Tokyo) for supporting this research project and to the authorities at the Photon Factory KEK for granting beamtime to this project under the proposal no. 90-231. The work also forms part of a project supplied by a European Community SCIENCE contract. We are indebted to N Sakai and H Shiotani for help with the experiments, and to S W Lovesey for discussions of the theory. The computer program for magnetic multiple scattering was adapted from one provided by N Sakai. The samples were made in the Department of Metallurgy and Materials of the University of Birmingham, UK.

References

[1] Cooper M J 1985 *Rep. Prog. Phys.* **48** 415
[2] Isaacs E D, McWhan D B, Peters C, Ice G E, Siddons D P, Hastings J B, Vettier C and Vogt O 1989 *Phys. Rev. Lett.* **62** 1671
[3] Sakai N, Terashima O and Sekizawa H 1984 *Nucl. Instrum. Methods* **221** 419
[4] Lipps F W and Tolhoek H A 1954 *Physica* **20** 85, 395
[5] Cooper M J, Zukowski E, Collins S P, Timms D N, Itoh F and Sakurai H 1992 *J. Phys.: Condens. Matter* **4** L399
[6] Timms D N, Zukowski E, Cooper M J, Laundy D, Collins S P, Itoh F, Sakurai H, Iwazumi T, Kawata H, Ito M, Sakai N, Tanaka Y and Sakurai Y 1993 *J. Phys. Soc. Japan* **62** 1716
[7] Fuess H, Givord D, Gregory A R and Schweizer J 1979 *J. Appl. Phys.* **50** 2000
[8] Brooks M S S, Nordström L and Johansson B 1991 *J. Phys.: Condens. Matter* **3** 2357
[9] Lander G H 1991 private communication
Gregory A R 1979 *PhD thesis* University of Frankfurt
[10] Lovesey S W 1990 private communication
[11] Campbell I A 1972 *J. Phys. F: Met. Phys.* **2** L47
[12] Boucherle J X, Schweizer J, Givord D, Gregory A and Schweizer J 1982 *J. Appl. Phys.* **53** 1950
[13] Brooks M S S, Eriksson O and Johansson B 1989 *J. Phys.: Condens. Matter* **1** 5861
[14] Kawata H, Miyahara T, Yamamoto S, Shioya T, Kitamura H, Sato S, Asaoka S, Kanaya N, Iida A, Mikuni A, Sato M, Iwazumi T, Kitajima Y and Ando M 1989 *Rev. Sci. Instrum.* **60** 1885
[15] Yamamoto S, Kawata H, Kitamura H and Ando M 1989 *Phys. Rev. Lett.* **62** 2672
[16] Kawata H, Sato M, Iwazumi T, Ando M, Sakai N, Ito M, Tanaka Y, Shiotani N, Itoh F, Sakurai H, Sakurai Y, Watanabe Y and Nanao S 1991 *Rev. Sci. Instrum.* **62** 2109
[17] Sakai N 1992 *Mat. Sci. Forum* **105–110** 431
[18] Tanaka Y, Sakai N, Kawata H and Iwazumi T 1992 *Rev. Sci. Instrum.* **63** 1213
[19] Ribberfors R 1975 *Phys. Rev.* B **12** 2067, 3136
[20] Sakai N 1987 *J. Phys. Soc. Japan* **56** 2477
[21] Biggs F, Mendelsohn L B and Mann J B 1975 *At. Data Nucl. Data Tables* **16** 201–309
[22] Burzo E 1971 *Z. Phys.* **32** 127
[23] Sakai N, Tanaka Y, Itoh F, Sakurai H, Kawata H and Iwazumi T 1991 *J. Phys. Soc. Japan* **60** 1201
[24] Zukowski E, Dobrzynski L, Cooper M J, Timms D N, Holt R S and Latuszkiewicz J 1990 *J. Phys.: Condens. Matter* **2** 6315
[25] Andrejczuk A, Dobrzynski L, Zukowski E, Cooper M J, Hamouda S and Latuszkiewicz J 1992 *J. Phys.: Condens. Matter* **4** 2735
[26] Cooper M J, Collins S P, Timms D N, Brahmia A, Kane P P, Holt R S and Laundy D 1988 *Nature* **333** 151